



Coplanar Circumbinary Planets Can Be Unstable to Large Tilt Oscillations in the Presence of an Inner Polar Planet

Anna C. Childs¹ , Rebecca G. Martin^{2,3} , Stephen Lepp^{2,3} , Stephen H. Lubow⁴ , and Aaron M. Geller¹ 

¹ Center for Interdisciplinary Exploration and Research in Astrophysics (CIERA) and Department of Physics and Astronomy Northwestern University, 1800 Sherman Ave., Evanston, IL 60201, USA; anna.childs@northwestern.edu

² Nevada Center for Astrophysics, University of Nevada, Las Vegas, NV 89154, USA

³ Department of Physics and Astronomy, University of Nevada, Las Vegas, 4505 South Maryland Parkway, Las Vegas, NV 89154, USA

⁴ Space Telescope Science Institute, 3700 San Martin Drive, Baltimore, MD 21218, USA

Received 2022 December 4; revised 2023 January 31; accepted 2023 February 17; published 2023 March 2

Abstract

Mutually misaligned circumbinary planets may form in a warped or broken gas disk or from later planet–planet interactions. With numerical simulations and analytic estimates we explore the dynamics of two circumbinary planets with a large mutual inclination. A coplanar inner planet causes prograde apsidal precession of the binary and the stationary inclination for the outer planet is higher for larger outer planet orbital radius. In this case a coplanar outer planet always remains coplanar. On the other hand, a polar inner planet causes retrograde apsidal precession of the binary orbit and the stationary inclination is smaller for larger outer planet orbital radius. For a range of outer planet semimajor axes, an initially coplanar orbit is librating meaning that the outer planet undergoes large tilt oscillations. Circumbinary planets that are highly inclined to the binary are difficult to detect—it is unlikely for a planet to have an inclination below the transit detection limit in the presence of a polar inner planet. These results suggest that there could be a population of circumbinary planets that are undergoing large tilt oscillations.

Unified Astronomy Thesaurus concepts: [Binary stars \(154\)](#); [Exoplanets \(498\)](#); [Exoplanet dynamics \(490\)](#); [Exoplanet astronomy \(486\)](#)

1. Introduction

While binary stars are ubiquitous in our Galaxy and over 5000 exoplanets have been found, only 41 circumbinary planets (CBPs) have been observed and confirmed thus far (NASA Exoplanet Archive 2022). The majority of these circumbinary planets are gas giants although a super-Earth as small as about $2 M_{\oplus}$ has been observed (Orosz et al. 2019) and are all in orbits that are nearly coplanar to the binary. The observed coplanarity is undoubtedly due to the difficulty of observing planets on highly misaligned orbits by current techniques (Schneider 1994; Martin & Triaud 2014; Martin 2017; Zhang & Fabrycky 2019; Martin & Fabrycky 2021). Based on considerations of disk evolution, if it is sufficiently fast, then we expect planets to be either coplanar or polar with respect to the binary orbit (e.g., Martin & Lubow 2017). While polar planets have not yet been found, there are several examples of polar disks (Kennedy et al. 2012, 2019; Kenworthy et al. 2022).

Polar circumbinary disks are more likely to be found around more eccentric binaries. Misaligned planets may form more easily around wider binaries where binary eccentricities are higher and the disk evolution is slower (e.g., Czekala et al. 2019). We show here, that under certain circumstances, circumbinary planets can reside on orbits that undergo large tilt oscillations. In effect, a coplanar planet can undergo tilt oscillations from coplanar to beyond polar, almost retrograde.

Around an eccentric binary, there are two types of nodal precession of a misaligned circumbinary test particle (Verrier &

Evans 2009; Farago & Laskar 2010; Doolin & Blundell 2011; Naoz 2016). An initially low inclination particle nodally precesses about the binary angular momentum vector (this is a circulating orbit). For high initial inclination, the particle can precess about the binary eccentricity vector (this is a librating orbit). The polar stationary inclination is the inclination where a particle does not undergo nodal precession and remains highly inclined. The stationary inclination for polar orbits is at 90° for all test particle semimajor axes. Prograde apsidal precession of the binary can be driven by general relativity (e.g., Naoz et al. 2017; Zanardi et al. 2018) or a triple star (e.g., Innanen et al. 1997; Morais & Correia 2012), and this leads to an increase in the polar stationary inclination with particle semimajor axis (Lepp et al. 2022, 2023). With apsidal precession of the binary, beyond a critical semimajor axis, all particle orbits are circulating and the particle behaves as it would around a circular orbit binary.

A gaseous circumbinary disk that is in good radial communication can undergo similar nodal precession to a test particle (e.g., Papaloizou & Terquem 1995; Larwood et al. 1996; Aly et al. 2015). Differential nodal precession as a function of distance in such a disk results in viscous dissipation. Viscous dissipation in a misaligned disk leads to evolution toward coplanar alignment or a stable polar configuration (Martin & Lubow 2017; Lubow & Martin 2018; Martin & Lubow 2018; Zanazzi & Lai 2018; Cuello & Giuppone 2019). Such misaligned circumbinary gas disks are often observed in nature and may result from the turbulent collapse of the molecular disk or from other mechanisms that later misalign the disk (Bonnell & Bastien 1992; Bate et al. 2010; Offner et al. 2010; Bate 2012; Tokuda et al. 2014; Bate 2018; Nealon et al. 2020).

If a disk is not in good radial communication, the torque from the binary can lead to disk warping or breaking (e.g., Facchini et al. 2013; Nixon et al. 2013). As a consequence of the breaking, an inner ring may then align (to polar or coplanar depending on its initial inclination and the binary eccentricity) on a shorter timescale than the outer parts of the disk (e.g., Lubow & Martin 2018; Smallwood et al. 2020). The radius at which the disk breaks depends on the disk properties (such as the aspect ratio and viscosity) and the binary properties, but for standard parameters the disk can break close to the binary (at radii less than about 10 times the binary semimajor axis) in both the viscous and wave-like regimes (Facchini et al. 2013; Nixon et al. 2013; Lubow & Martin 2018). Another mechanism that may result in CBP misalignment involves multiple accretion events onto a binary that can form misaligned disks (Bate 2018).

Theoretical studies suggest that planet formation in polar circumbinary disks can take similar pathways as planet formation in coplanar circumbinary disks (Childs & Martin 2021a, 2021b, 2022). Giant planets that form in a warped or broken disk may form with a mutual misalignment. The misalignment could also arise from later planet–planet or planet–binary interactions (Chen et al. 2022).

In this Letter we investigate the dynamics of a two planet circumbinary system in which the planets have a mutual misalignment. Understanding the dynamics of such a system will aid in future observations. Polar planets present additional challenges for detection than coplanar planets. However, unique detectable dynamical signatures of coplanar planets that result from interactions with inner polar planets may provide indirect detections of polar planets. In Section 2 we present numerical simulations of the four-body system. We show that there is a range of semimajor axes for which an initially coplanar outer planet is librating and undergoing large tilt oscillations. In Section 3 we provide an analytic framework to find the stationary inclination of an outer planet with an inner circumbinary planetary companion and the range of semimajor axes for which the outer planet librates. We show good agreement with our numerical simulations. Finally, in Section 4 we conclude with a summary of our findings.

2. Numerical Simulations

To model the dynamics of the four-body system we use the n -body code REBOUND (Rein & Liu 2012) with the WHFAST integrator (Rein & Tamayo 2015). We include the effects of general relativity (GR) by using the “gr_full” module from REBOUNDX (Tamayo et al. 2020),⁵ but we find their effects to be small. The binary is composed of two equal mass stars, $m_1 = m_2 = 0.5 M_\odot$ with a total mass of $m_b = m_1 + m_2 = 1 M_\odot$. They are in an orbit with semimajor axis $a_b = 0.5$ au with an eccentricity of $e_b = 0.8$. We vary the mass, m_{p1} , and initial inclination, i_{p1} , of the inner planet but keep it at a fixed semimajor axis of $a_{p1} = 5 a_b$. For the outer planet, we vary the semimajor axis, a_{p2} , and inclination, i_{p2} , but fix the mass to a small value of $m_{p2} = 1 \times 10^{-10} M_\oplus$. Such a small mass does not affect the dynamics of the four-body system. Moreover, there is little difference in the behavior if we instead use a Jupiter-mass outer planet or a different binary mass fraction

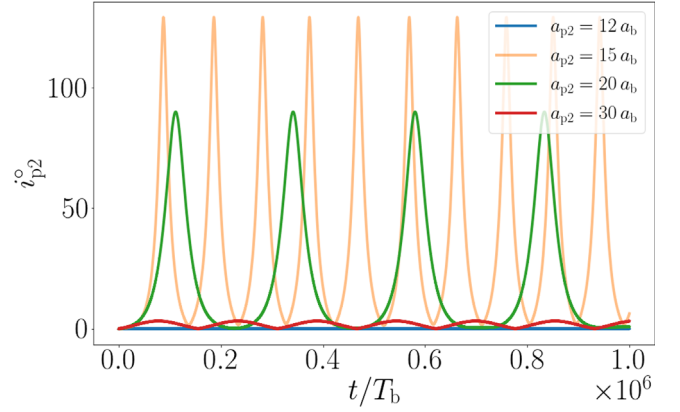


Figure 1. Numerical results for the inclination evolution of an outer planet orbiting an equal mass binary star with binary eccentricity $e_b = 0.8$ with an inner Jupiter-mass polar planet orbiting with semimajor axis $a_{p1} = 5 a_b$. The outer planet begins coplanar to the binary orbit with $i_{p2} = 0^\circ$ for different outer planet semimajor axis.

(see also Chen et al. 2019; Martin & Lubow 2019). Both planets are in initially circular orbits.

We measure all orbital elements in the frame of the binary. The inclination of a body is defined as

$$i = \cos^{-1}(\hat{l}_b \cdot \hat{l}_p), \quad (1)$$

where $\hat{\cdot}$ denotes a unit vector, \mathbf{l}_b is the binary angular momentum vector, and \mathbf{l}_p is the planet angular momentum. The nodal phase angle of a planet is calculated with

$$\phi = \tan^{-1} \left(\frac{\hat{l}_p \cdot (\hat{l}_b \times \hat{e}_b)}{\hat{l}_p \cdot \hat{e}_b} \right) + \frac{\pi}{2}, \quad (2)$$

where \hat{e}_b is the eccentricity vector of the binary (Chen et al. 2019). Initially we take $\phi_{p1} = \phi_{p2} = 90^\circ$.

We first follow the inclination evolution of an outer planet with an inner polar planet companion that has the mass of Jupiter. Figure 1 shows the inclination of the outer planet over one million binary orbits (T_b). The planet has an initial inclination of $i_{p2} = 0^\circ$ and we simulate the system at four different semimajor axes for the outer planet. With $a_{p2} = 12 a_b$, the planet remains nearly coplanar, although its inclination immediately jumps to about 0.1° and then slightly oscillates about this inclination. This inclination is above the transit detection limit and, even for this small tilt, the planet spends about 94% of its time above the transit detection limit for an eclipsing binary (Li et al. 2016). When the planet is farther out at $15 a_b$ and $20 a_b$, it undergoes large tilt oscillations. In these cases, after the initial evolution, the planet inclination never drops sufficiently for the planet to be detectable by periodic transits. For even larger outer planet semimajor axis, $a_{p2} = 30 a_b$, the tilt oscillations are smaller. However, such a planet never has a small enough inclination to be below the transit detection limit even though it remains close to coplanar.

Figure 2 shows $i_{p2} \cos \phi_{p2} - i_{p2} \sin \phi_{p2}$ phase diagrams for various semimajor axes of the outer planet and inclinations of the inner planet. The inner planet has a fixed mass of $m_{p1} = 1 M_{\text{Jup}}$ for each phase diagram. The green and blue lines show circulating orbits with initial inclinations less than and greater than 90° , respectively. The red and cyan lines show librating orbits with initial inclinations less than and greater than 90° , respectively.

⁵ The n -body simulation results can be reproduced with the REBOUND code (Astrophysics Source Code Library identifier [ascl.net/1110.016](https://www.ascl.net/1110.016)) and the REBOUNDX code (Astrophysics Source Code Library identifier [ascl.net/2011.020](https://www.ascl.net/2011.020)).

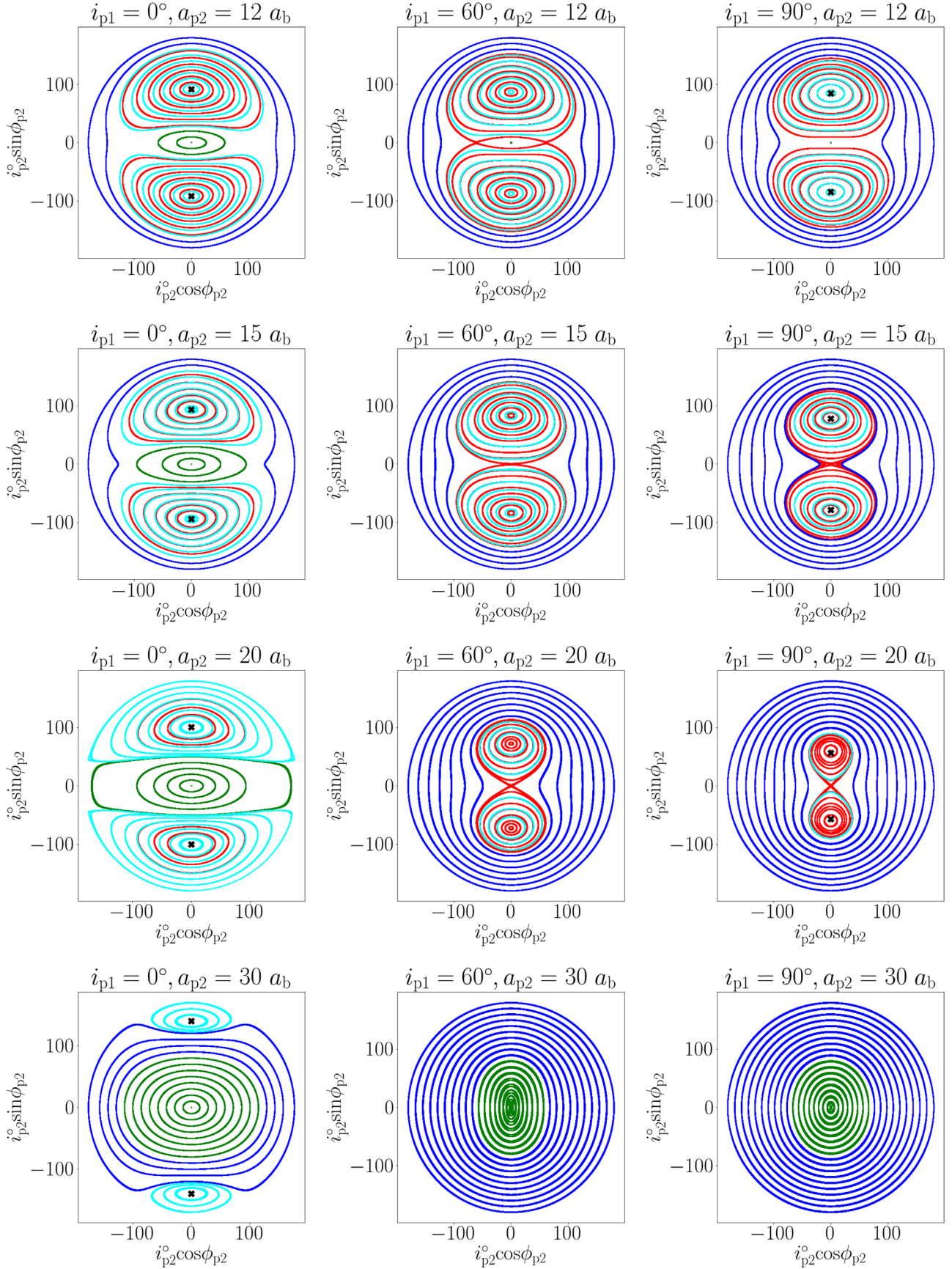


Figure 2. Phase diagrams for various semimajor axes of the outer planet and inclinations of the inner planet. Green and blue orbits are circulating orbits with initial inclinations less than and greater than 90° , respectively. Red and cyan orbits are librating orbits with initial inclinations less than and greater than the stationary polar inclination, respectively. The black crosses show the stationary polar inclination found with Equation (8).

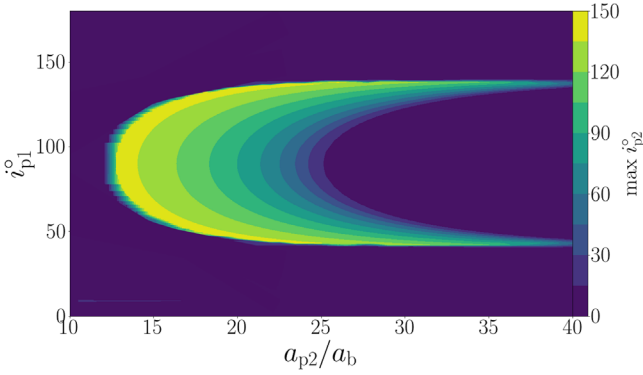


Figure 3. Contour plot of the maximum inclination of the outer planet as a function of the outer planet semimajor axis and the initial inclination of the inner Jupiter-mass planet. The outer planet has an initial inclination of 0° .

For an inner planet that is coplanar (left panels of Figure 2), a coplanar outer planet always remains coplanar. There are always circulating orbits for initial inclinations of the outer planet that are close to coplanar. For larger values of the outer planet semimajor axis, the stationary polar inclination is larger and so is the range of initial inclinations for circulating orbits. Outside of a critical radius, the librating orbits disappear and the only possible orbits are circulating. This is a result of the prograde precession of the binary that is driven by the inner planet. This is similar to the case of GR driven apsidal precession (Lepp et al. 2022) except that the timescale for the precession may be much shorter in this case and therefore the critical radius is smaller.

For a polar inner planet (right panels of Figure 2), the binary undergoes retrograde nodal precession. The stationary polar inclination is smaller for larger semimajor axis of the outer planet. The critical inclination that separates the circulating and librating orbits also is smaller and the possibility for a coplanar orbit is removed for sufficiently large semimajor axis. This can be seen in the two middle panels on the right-hand side where an initially coplanar orbit is librating! The initially coplanar outer planet undergoes large tilt oscillations. For even larger semimajor axis, all possible orbits become circulating. Similar behavior can also be seen in the middle panels for an inner planet inclination of $i_{p1} = 60^\circ$.

Figure 3 shows how the inclination of a Jupiter-mass inner planet affects the maximum inclination of the outer planet, which begins coplanar, over one million binary orbits as a function of the outer planet’s distance. If the outer planet is closer in than $12 a_b$ the outer planet remains coplanar regardless of the inner planet’s inclination. This is because the dynamics of the outer planet here are dominated by the dynamics of the binary, and the outer planet precesses with the binary. Exterior to $12 a_b$ however, the outer planet can be librating, and therefore its maximum inclination can be very large. This occurs for inner planet inclination in the approximate range of 40° – 130° . For larger outer planet semimajor axis, the planet again remains coplanar since it no longer precesses with the binary. The distance at which this happens depends strongly on the inner planet inclination.

3. Analytic Estimates

We now use an analytic model to find the critical semimajor axes at which the outer planet orbital dynamics changes in the presence of an inner polar planet. The outer planet is modeled

as a test particle and both planets are in initially circular orbits. We make the approximation that the gravitational effects of the inner planet on the outer planet are ignored. The inner planet interacts with the binary and causes it to precess. The test particle experiences the gravitational effects of the binary only. We examine the accuracy of this approximation below. In addition we consider only effects that arise in the quadrupole approximation for the gravitational forcing by the binary. The circumbinary planet orbit remains nearly circular because its eccentricity is constant in time in the quadrupole approximation (Farago & Laskar 2010). This quadrupole approximation for the binary is justified because octupole terms vanish for a circular orbit circumbinary planet (e.g., Equation (7) of de Elía et al. 2019).

The nodal precession of the outer planet is described by

$$\dot{\phi}_{p2} = \dot{\phi}_{p2,\text{binary}} - \dot{\omega}_b. \quad (3)$$

The time evolution of the nodal precession of the test particle orbiting around an eccentric binary up to the quadrupole level of secular approximation is

$$\dot{\phi}_{p2,\text{binary}} = -\frac{3}{4}\Omega_b \frac{m_1 m_2}{m_b^2} \left(\frac{a_b}{a_{p2}}\right)^{7/2} F_1, \quad (4)$$

where the orbital frequency of the binary is $\Omega_b = \sqrt{Gm_b/a_b^3}$ and we define

$$F_1 = \cos i_{p2} \left[1 + \frac{3}{2}e_b^2 - \frac{5}{2}e_b^2 \cos 2\phi_{p2} \right] \quad (5)$$

(e.g., Innanen et al. 1997; Kiseleva et al. 1998; Naoz et al. 2017; Zanardi et al. 2018).

The binary undergoes apsidal precession driven by the inner planet. The precession rate of the longitude of periastron of the binary in the limit of a small mass companion is

$$\dot{\omega}_b = \frac{3}{4}\Omega_b \frac{m_{p1}}{m_b} \left(\frac{a_b}{a_{p1}}\right)^3 F_2, \quad (6)$$

where

$$F_2 = (1 - e_b^2)^{-1/2} [2 - 2e_b^2 + 5(e_b^2 - \sin^2 i_{p1}) \sin^2 \omega_b - \cos i_{p1} (1 - e_b^2 + 5e_b^2 \sin^2 \omega_b)], \quad (7)$$

(e.g., Innanen et al. 1997; Naoz 2016) and the argument of periastron of the binary is ω_b .

We find the polar stationary inclination of the outer planet (by setting $\dot{\phi}_{p2} = 0$ and $\phi_{p2} = 90^\circ$) to be

$$\cos i_s = -\frac{m_{p1} m_b}{m_1 m_2} \left(\frac{a_{p2}}{a_b}\right)^{7/2} \left(\frac{a_b}{a_{p1}}\right)^3 \frac{F_2}{1 + 4e_b^2}. \quad (8)$$

For a coplanar inner planet, $i_{p1} = 0^\circ$, the value of ω_b does not matter because those terms cancel out to give $F_2 = (1 - e_b^2)^{1/2}$. For a polar inner planet, $i_{p1} = 90^\circ$, $\omega_b = 90^\circ$, and we find $F_2 = -3(1 - e_b^2)^{1/2}$ (see also Zhang & Fabrycky 2019). The black crosses in Figure 2 show that Equation (8) accurately predicts the stationary polar inclination for a two circumbinary system with $i_{p1} = 0^\circ$ and 90° . For the $i_{p1} = 90^\circ$ system, for larger semimajor axis of the outer planet, the stationary inclination is slightly higher than the analytical predictions. This small offset can be attributed to GR effects

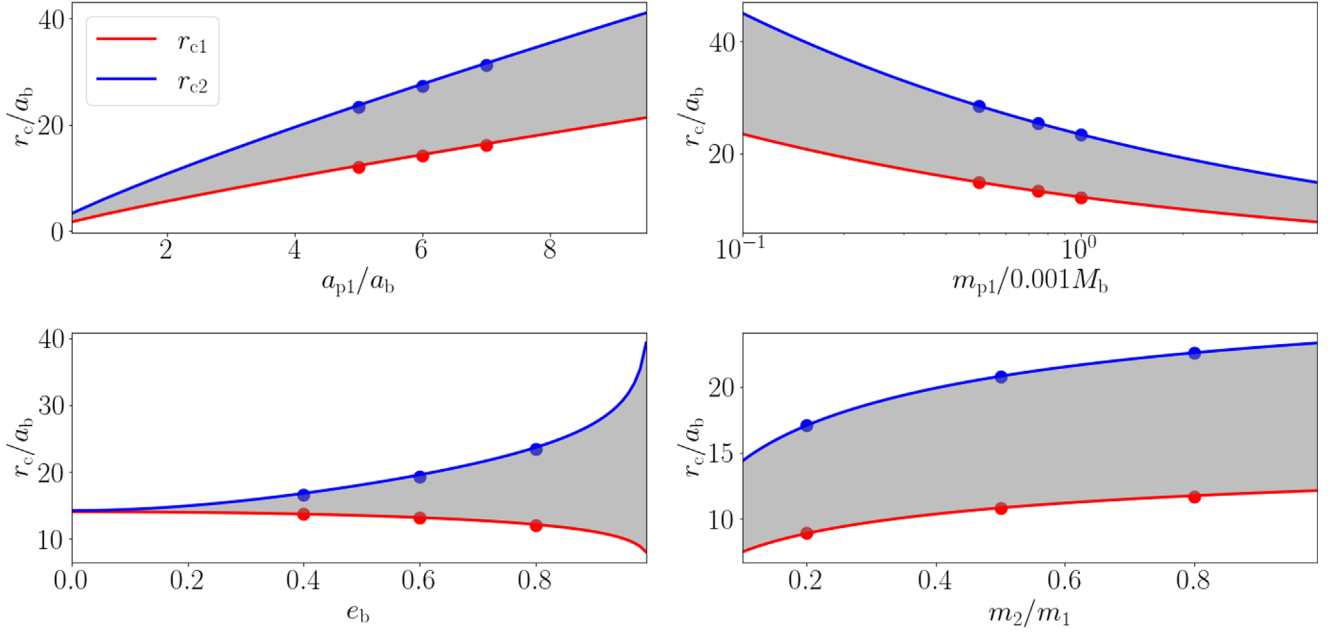


Figure 4. Critical radii as a function of a_{p1} (top left), m_{p1} (top right), e_b (lower left), and m_2/m_1 (lower right). The default parameters from our numerical solutions are used for all other parameters besides the parameter we vary in each panel. The red and blue lines mark r_{c1} and r_{c2} (Equations (9) and (10), respectively). The gray shaded region between these two curves denotes where an initially coplanar outer planet is librating with an inner polar planet. The points show our numerical results.

included in the simulations that are not accounted for in our analytic expressions and use of the quadrupole approximation of the potential in the analytic model.

Now we consider the critical a_{p2} where the librating orbits reach an inclination of 0° (by setting $i_{p2} = \phi_{p2} = 0^\circ$ and $\dot{\phi}_{p2} = 0$) to be

$$r_{c1} = \left[\left(\frac{a_{p1}}{a_b} \right)^3 \frac{m_1 m_2}{m_{p1} m_b} \frac{(1 - e_b^2)}{(-F_2)} \right]^{2/7} a_b. \quad (9)$$

For the polar inner planet parameters, this is $r_{c1} = 12.1 a_b$, in agreement with the right-hand panels of Figures 2 and 3. There is also a critical radius outside of which there are no librating orbits ($i_{p2} = 0^\circ$, $\phi_{p2} = 90^\circ$ and $\dot{\phi}_{p2} = 0^\circ$) given by

$$r_{c2} = \left[\left(\frac{a_{p1}}{a_b} \right)^3 \frac{m_1 m_2}{m_{p1} m_b} \frac{(1 + 4e_b^2)}{(-F_2)} \right]^{2/7} a_b. \quad (10)$$

For the polar inner planet parameters we find $r_{c2} = 23.4 a_b$, in agreement with the right-hand panels in Figures 2 and 3. Now if a coplanar outer planet has a radius in the range $r_{c1} < a_{p2} < r_{c2}$, then it is in a librating orbit. A planet that is initially coplanar with the binary at a larger orbital radius than the outer critical radius r_{c2} or a smaller radius than the inner critical radius r_{c1} is on a circulating orbit about the binary, provided that it is not too close to the binary.

Figure 4 shows how these critical radii change as a function of a_{p1} , m_{p1} , e_b , and m_2/m_1 . The default values from our numerical solutions are used for all other parameters in addition to the parameter we vary in each panel. The parameters are $a_{p1} = 5 a_b$, $m_{p1} = 0.001 m_b$, $e_b = 0.8$ and $m_2/m_1 = 1$. The radial range for an outer librating planet that is initially coplanar increases significantly with binary eccentricity. The radius is larger for larger inner planet semimajor axis and smaller with the inner planet mass. The critical radii are relatively insensitive to the binary mass fraction. We numerically find the critical

radii and plot these numerical values on Figure 4 with points. We find good agreement for r_{c1} and r_{c2} with our analytic predictions and the location of these points are insensitive to the effects of GR in the parameter space sampled.

To ensure our predictions are applicable to circumbinary systems, we estimate the disk breaking radius using Equation (34) of Lubow & Martin (2018). Assuming the fiducial disk parameters of Lubow & Martin (2018), a disk aspect ratio of $H/R = 0.05$, and our binary parameters, the disk breaking radius is $r_{\text{break}} \approx 2.8 a_b$. This is in agreement with simulations of similar disks (Martin & Lubow 2018; Abod et al. 2022). This disk breaking radius may permit the existence of an inner highly misaligned planet ($a_{p1} \lesssim 2.8 a_b$) and an outer planet beyond r_{c1} ($a_{p1} \gtrsim 12 a_b$).

We consider the accuracy of our approximation that ignores the gravitational effects of the inner planet on the outer planet. The ratio R of the nodal precession of the outer planet that is caused by the inner planet to the nodal precession rate of the outer planet that is caused by the binary is estimated by using Equation (4) as

$$R = \frac{m_{p1} m_b}{m_1 m_2} \left(\frac{a_{p1}}{a_b} \right)^2 \frac{\tan(i_{p2})}{1 + \frac{3}{2} e_b^2}, \quad (11)$$

where we have adapted Equation (4) for the inner planet to the case of a “binary” consisting of the inner planet and the central binary as a point mass. Note that R is independent of a_{p2} . For the parameters adopted in this paper, $R \simeq 0.05 \tan i_{p2}$. Therefore, for most tilt angles of the outer planet, the nodal precession of the outer planet is dominated by the effects of the binary. We also made a direct numerical test of this approximation by running the model with $a_{p2} = 15 a_b$ in which the gravitational forcing of the outer planet due to the inner planet is ignored and compared the result to the case in which that forcing is included. We find that the difference in $i_{p2}(t)$ for

these two cases is small, $<1\%$, which justifies our approximation.

4. Conclusions



Using numerical and analytical methods we have explored the dynamics of two mutually misaligned circumbinary planets. We focused on a polar inner planet and an initially coplanar outer planet. Such a configuration could arise from disk evolution. We treat the outer planet as a test particle and allow the inner planet to have a range of masses. Based on our tests, the properties of the outer particle well represent the properties of a planet. We find that the inner planet drives apsidal precession of the binary, at a faster rate than GR, which affects the dynamics of the outer planet.

A polar inner planet causes retrograde apsidal precession of the binary orbit and the stationary inclination is smaller for larger outer planet semimajor axis. There is a range of semimajor axis for the outer planet for which an outer planet that is initially coplanar with the binary is on a librating orbit and therefore undergoes large tilt oscillations (see Figure 1). Outside this range of radii, a planet that is initially coplanar with the binary is on a circulating orbit. The radial extent of the librating region increases with larger inner planet semimajor axis, binary eccentricity, and mass ratio, and decreases with the mass of the inner planet. With an inner polar planet, an outer planet that begins close to coplanar with the binary may spend only a small fraction of its time with an inclination small enough to be detected by periodic transits. Planets that are undergoing large tilt oscillations may never have a small enough inclination to be detected in this way.

We predict that there is a large radial region where initially nearly coplanar orbits to the binary undergo large tilt oscillations, if there is an inner highly misaligned companion. Transit detection techniques are strongly biased against finding such highly misaligned CBPs. These results can help constrain occurrence rates of, and aid future observations of highly misaligned CBPs.

A.C.C. and A.M.G. acknowledge support from the NSF through grant NSF AST-2107738. R.G.M. and S.H.L. acknowledges support from NASA through grants 80NSSC19K0443 and 80NSSC21K0395. S.H.L. thanks the Institute for Advanced Study for visitor support.

ORCID iDs

Anna C. Childs  <https://orcid.org/0000-0002-9343-8612>
 Rebecca G. Martin  <https://orcid.org/0000-0003-2401-7168>
 Stephen Lepp  <https://orcid.org/0000-0003-2270-1310>
 Stephen H. Lubow  <https://orcid.org/0000-0002-4636-7348>
 Aaron M. Geller  <https://orcid.org/0000-0002-3881-9332>

References

- Abod, C. P., Chen, C., Smallwood, J., et al. 2022, *MNRAS*, 517, 732
 Aly, H., Dehnen, W., Nixon, C., & King, A. 2015, *MNRAS*, 449, 65
 Bate, M. R. 2012, *MNRAS*, 419, 3115
 Bate, M. R. 2018, *MNRAS*, 475, 5618
 Bate, M. R., Lodato, G., & Pringle, J. E. 2010, *MNRAS*, 401, 1505
 Bonnell, I., & Bastien, P. 1992, *ApJ*, 401, 654
 Chen, C., Franchini, A., Lubow, S. H., & Martin, R. G. 2019, *MNRAS*, 490, 5634
 Chen, C., Lubow, S. H., & Martin, R. G. 2022, *MNRAS*, 510, 351
 Childs, A. C., & Martin, R. G. 2021a, *MNRAS*, 507, 3461
 Childs, A. C., & Martin, R. G. 2021b, *ApJL*, 920, L8
 Childs, A. C., & Martin, R. G. 2022, *ApJL*, 927, L7
 Cuello, N., & Giuppone, C. A. 2019, *A&A*, 628, A119
 Czekala, I., Chiang, E., Andrews, S. M., et al. 2019, *ApJ*, 883, 22
 de Elía, G. C., Zanardi, M., Dugaro, A., & Naoz, S. 2019, *A&A*, 627, A17
 Doolin, S., & Blundell, K. M. 2011, *MNRAS*, 418, 2656
 Facchini, S., Lodato, G., & Price, D. J. 2013, *MNRAS*, 433, 2142
 Farago, F., & Laskar, J. 2010, *MNRAS*, 401, 1189
 Innanen, K. A., Zheng, J. Q., Mikkola, S., & Valtonen, M. J. 1997, *AJ*, 113, 1915
 Kennedy, G. M., Matrà, L., Facchini, S., et al. 2019, *NatAs*, 3, 230
 Kennedy, G. M., Wyatt, M. C., Sibthorpe, B., et al. 2012, *MNRAS*, 421, 2264
 Kenworthy, M. A., González Picos, D., Elizondo, E., et al. 2022, *A&A*, 666, A61
 Kiseleva, L. G., Eggleton, P. P., & Mikkola, S. 1998, *MNRAS*, 300, 292
 Larwood, J. D., Nelson, R. P., Papaloizou, J. C. B., & Terquem, C. 1996, *MNRAS*, 282, 597
 Lepp, S., Martin, R. G., & Childs, A. C. 2022, *ApJL*, 929, L5
 Lepp, S., Martin, R. G., & Lubow, S. H. 2023, *ApJ*, 943, L4
 Li, G., Holman, M. J., & Tao, M. 2016, *ApJ*, 831, 96
 Lubow, S. H., & Martin, R. G. 2018, *MNRAS*, 473, 3733
 Martin, D. V. 2017, *MNRAS*, 465, 3235
 Martin, D. V., & Fabrycky, D. C. 2021, *AJ*, 162, 84
 Martin, D. V., & Triaud, A. H. M. J. 2014, *A&A*, 570, A91
 Martin, R. G., & Lubow, S. H. 2017, *ApJ*, 835, L28
 Martin, R. G., & Lubow, S. H. 2018, *MNRAS*, 479, 1297
 Martin, R. G., & Lubow, S. H. 2019, *MNRAS*, 490, 1332
 Morais, M. H. M., & Correia, A. C. M. 2012, *MNRAS*, 419, 3447
 Naoz, S. 2016, *ARA&A*, 54, 441
 Naoz, S., Li, G., Zanardi, M., de Elía, G. C., & Di Sisto, R. P. 2017, *AJ*, 154, 18
 NASA Exoplanet Archive 2022, Planetary Systems, Version: 2022-11-15 10:00, NExSci-Caltech/IPAC, doi:10.26133/NEA12
 Nealon, R., Cuello, N., & Alexander, R. 2020, *MNRAS*, 491, 4108
 Nixon, C., King, A., & Price, D. 2013, *MNRAS*, 434, 1946
 Offner, S. S. R., Kratter, K. M., Matzner, C. D., Krumholz, M. R., & Klein, R. I. 2010, *ApJ*, 725, 1485
 Orosz, J. A., Welsh, W. F., Haghighipour, N., et al. 2019, *AJ*, 157, 174
 Papaloizou, J. C. B., & Terquem, C. 1995, *MNRAS*, 274, 987
 Rein, H., & Liu, S. F. 2012, *A&A*, 537, A128
 Rein, H., & Tamayo, D. 2015, *MNRAS*, 452, 376
 Schneider, J. 1994, *P&SS*, 42, 539
 Smallwood, J. L., Franchini, A., Chen, C., et al. 2020, *MNRAS*, 494, 487
 Tamayo, D., Rein, H., Shi, P., & Hernandez, D. M. 2020, *MNRAS*, 491, 2885
 Tokuda, K., Onishi, T., Saigo, K., et al. 2014, *ApJL*, 789, L4
 Verrier, P. E., & Evans, N. W. 2009, *MNRAS*, 394, 1721
 Zanardi, M., de Elía, G. C., Di Sisto, R. P., & Naoz, S. 2018, *A&A*, 615, A21
 Zanazzi, J. J., & Lai, D. 2018, *MNRAS*, 473, 603
 Zhang, Z., & Fabrycky, D. C. 2019, *ApJ*, 879, 92